Earth and Planetary Science Letters 278 (2009) 257–266

Contents lists available at ScienceDirect

Earth and Planetary Science Letters

journal homepage: www.elsevier.com/locate/epsl

Contrasting compositions of Saharan dust in the eastern Atlantic Ocean during the last deglaciation and African Humid Period

Jennifer M. Cole [a,*], Steven L. Goldstein [a,b], Peter B. deMenocal [a,b], Sidney R. Hemming [a,b], Francis E. Grousset [a,c]

[a] Lamont-Doherty Earth Observatory, Columbia University, Palisades, NY 10964, USA
[b] Department of Earth and Environmental Sciences, Columbia University, Palisades, NY 10964, USA
[c] Université de Bordeaux, CNRS UMR 5805 EPOC, Avenue des Facultés, 33405 Talence, France

ARTICLE INFO

Article history:
Received 9 June 2008
Received in revised form 12 October 2008
Accepted 7 December 2008
Available online 23 January 2009

Editor: M.L. Delaney

Keywords:
Saharan dust
Sr and Nd isotopes
provenance
weathering
African Humid Period
ODP Site 658

ABSTRACT

During the African Humid Period (AHP), much of the modern hyperarid Saharan desert was vegetated and covered with numerous lakes. In marine sediments off northwestern Africa, the AHP is represented by markedly reduced siliciclastic sediment flux between ~12.3 and 5.5 ka. Changes in the origin of this terrigenous sediment fraction can be constrained by sediment chemistry and radiogenic isotope tracers. At Ocean Drilling Program (ODP) Site 658, Hole C (20°44.95′N, 18°34.85′W, 2263 mbsl), the neodymium (Nd) isotope composition of terrigenous detritus shows little variability throughout the last 25 kyr, indicating that the contributing geological terranes have not changed appreciably since the last glacial period. In contrast, there were large and abrupt changes in strontium (Sr) isotope ratios and chemical compositions associated with the AHP, during which $^{87}Sr/^{86}Sr$ ratios were markedly less radiogenic, and sediments show higher chemical indices of alteration. We show that sediment geochemical changes during the AHP cannot be attributed to changes in the source terranes, physical sorting, or intensity of chemical weathering. The low $^{87}Sr/^{86}Sr$ and high Sr concentrations of AHP-age samples also conflict with the interpretation of increased fine-grained, fluvially derived sediments. We propose that the most significant compositional changes at ODP 658C are due to the addition of an aluminosilicate component that has a highly altered major element signature but is enriched in soluble elements like Sr and magnesium (Mg) compared to aluminum (Al) and has low $^{87}Sr/^{86}Sr$ relative to local terrigenous source areas. We interpret these characteristics to reflect authigenic sediment supply from extensive North African paleolake basins that were prevalent during the AHP.

1. Introduction

On glacial to interglacial time scales, northern Africa fluctuated between arid to hyperarid conditions, such as the late Holocene and the Last Glacial Maximum (LGM), and much wetter conditions, called African humid periods. These humid to arid shifts have been documented in terrestrial records of fossil mammals (McIntosh and McIntosh, 1983) and ancient lake highstands (Street and Grove, 1979), and in marine records of fossil pollen (Hooghiemstra et al., 2006) and sediment compositions (deMenocal et al., 2000a; deMenocal et al., 2000b; Tjallingii et al., 2008). During these humid periods the Saharan desert region was nearly completely vegetated (Jolly et al., 1998) with numerous lakes (Gasse, 2000; Hoelzmann et al., 1998). The most recent African Humid Period (AHP) occurred roughly between ~9 and 6 ka (Ritchie et al., 1985), but continuous, high-resolution marine sediment records indicate a more extended duration of the wettest part of the AHP from about 12.3 to 5.5 ka (Adkins et al., 2006; deMenocal et al., 2000b).

In the present day, the Saharan region is the world's greatest source of mineral dust to the atmosphere (Prospero et al., 2002), with nearly half a billion tons exported annually (Schütz et al., 1981). Changes in Saharan dust supply can be related to changes in precipitation, especially droughts, which lead to reduced vegetation, allowing for increased wind deflation of soils and ephemeral stream and lake deposits (Prospero and Nees, 1977). Thus dust deposition in the Atlantic today is higher than during the last AHP, but in many locations it was higher by a factor of two to five during the LGM compared to the present day (Bradtmiller et al., 2007; Kohfeld and Harrison, 2001; Ruddiman, 1997).

Many factors, such as changes in wind intensity, direction, and seasonality, as well as vegetation cover, terrestrial weathering intensity, and balance between aeolian and fluvial transport, affect the composition of terrestrial material that is ultimately deposited in deep-sea sediments off Northwest Africa. Strontium (Sr) and neodymium (Nd) isotopic variations produced by long-lived radioactive decay have shown to be a powerful tool for the study of provenance of silicate detritus in marine sediment cores (e.g., Ahmad et al., 2005; Cullen et al., 2000; Eisenhauer et al., 1999; Franzese et al.,

* Corresponding author. Tel.: +1 270 745 0692; fax: +1 845 365 8155.
E-mail address: jcole@ldeo.columbia.edu (J.M. Cole).

0012-821X/$ – see front matter © 2008 Elsevier B.V. All rights reserved.
doi:10.1016/j.epsl.2008.12.011

2006; Grousset and Biscaye, 2005; Grousset et al., 1998; Grousset et al., 1992; Jullien et al., 2007; Jung et al., 2004; Latimer et al., 2006; Nakai et al., 1993; Pettke et al., 2000; Rutberg et al., 2005; Tütken et al., 2002; Walter et al., 2000; Weldeab et al., 2002). Recently it has been suggested that variations in Sr isotopes in marine sediments off eastern Africa (Jung et al., 2004) and in the Bay of Bengal (Colin et al., 2006) reflect changes in terrestrial weathering régimes. In addition to radiogenic isotope tracers, major and trace element concentrations and ratios in marine sediments can also be used to track changes in provenance, transport mechanisms, and weathering histories (e.g., Colin et al., 2006; Jullien et al., 2007; Matthewson et al., 1995; McLennan et al., 1993; Sirocko et al., 2000; Zabel et al., 2003).

Here we present major and trace element chemistry and Sr and Nd isotopes of the terrigenous fraction in sediments from Ocean Drilling Program (ODP) Site 658C deposited over the past ~25 kyr to study the relationship between terrestrial climate changes and marine sediment provenance. We investigate whether geochemical variations are best interpreted in terms of changes in geologic source terrane, physical sorting of sediments, intensity of chemical weathering, or some other cause.

1.1. Site location and sedimentation history

ODP 658C was drilled on the continental slope off Northwest Africa, 160 km off Cap Blanc, Mauritania (20°44.95′N, 18°34.85′W, 2263 mbsl; Fig. 1) (Ruddiman et al., 1988). Sedimentation rates in the section of core studied here were previously determined at approximately 18 cm/kyr (deMenocal et al., 2000a) due to the position directly under the boreal summer Saharan dust plume and within a permanent wind-driven upwelling zone (Sarnthein and Tiedemann, 1989). The last 23 kyr (~415 cm) of the record were constrained by 30 AMS 14-carbon (^{14}C) dates and we utilize that age-model in this study (deMenocal et al., 2000b). A hiatus was identified between 328 and 324 cm depth, corresponding to 17.4 to 14.8 ka.

deMenocal et al. (2000a) sampled this core at high-resolution (2 cm intervals equaling ~50 to ~100 years) for sedimentology (carbonate, biogenic opal, and terrigenous percentages), benthic foraminiferal stable isotopes, and faunally derived sea surface temperatures over the past 23 kyr. During Marine Isotope Stage 2 (subsequently referred to as the LGM) and latest Holocene, sediments were ~55–60% terrigenous (i.e. total minus the sum of carbonate and biogenic opal), while during the AHP, sediments were only about 40–45% terrigenous (Fig. 2). Carbonate and opal are not considered be major components of terrigenous material, as Saharan dusts tend to be dominated by aluminosilicates (illite/mica) and quartz, with less than ~10% calcite (e.g., Glaccum and Prospero, 1980). Freshwater diatoms are present in aeolian material (e.g., Pokras and Mix, 1985), but they do not dominate the marine opal fraction (e.g., Lange et al., 1998). Three shifts with a magnitude of greater than 10% in the relative amount of terrigenous sediment occur at 14.8 ka, 12.3 ka, and 5.5 ka, corresponding to the onset of the AHP, the termination of the Younger Dryas, and the termination of the AHP, respectively, (deMenocal et al., 2000a). All three transitions are abrupt, lasting only decades to a few centuries. deMenocal et al. (2000a) showed that the timing of the transitions into and out of the AHP are coincident with the crossing of "threshold values" in boreal summer season insolation and relate to non-linear responses of the West African monsoon system (Claussen et al., 1999; deMenocal et al., 2000a).

Adkins et al. (2006) used the quantitative constant flux proxy 230-thorium-excess (^{230}Th$_{xs}$) (e.g., Bacon, 1984) to calculated carbonate, opal, and terrigenous flux records for the last 20 kyr for this core. Normalized terrigenous fluxes (Fig. 2) were high for the late Holocene and LGM and were markedly lower during the AHP, consistent with high and low percentages of terrigenous component. The fluxes, like the percent terrigenous fractions, show abrupt transitions between these régimes. During the Younger Dryas the ^{230}Th$_{xs}$ normalized terrigenous flux was higher than the late Holocene, in contrast to a lower percentage of terrigenous material (Adkins et al., 2006). Therefore, Th-based flux data show that the wettest interval of the AHP occurred between about 12.3 and 5.5 ka, and we subsequently refer to the AHP as the period between 12.3 and 5.5 ka.

1.2. Climatic setting

North African climate zones range from equatorial rainforests to subtropical hyperarid deserts. Associated with boreal summer heating, the Intertropical Convergence Zone (ITCZ) attains its most northerly position centered near 20°N and draws moist maritime air from the

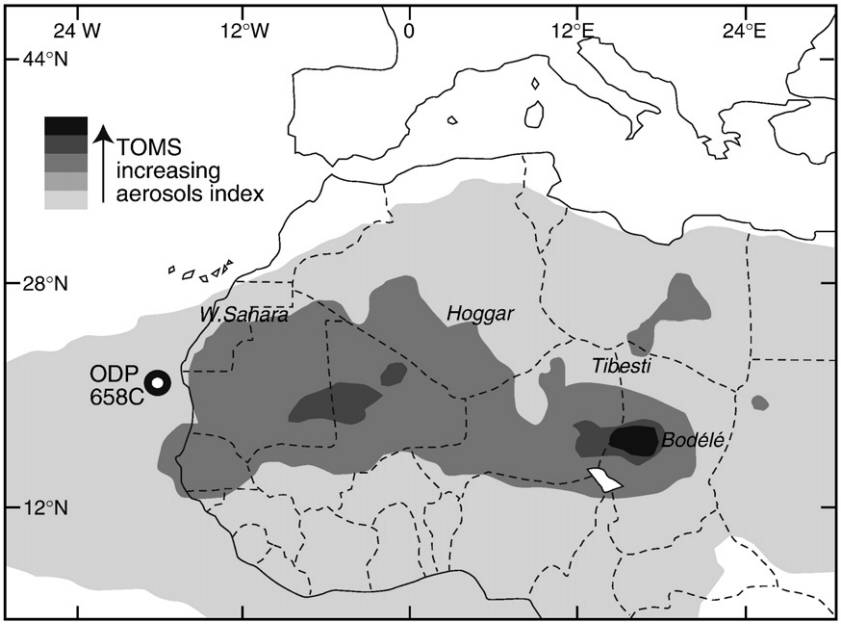

Fig. 1. Map showing sampling location of ODP 658C and the TOMS 13-year (1992–2005) averaged aerosol concentrations (http://toms.gsfc.nasa.gov/aerosols/aerosols_v8.html) modified from Moreno et al. (2006). The area of highest aerosol concentration is the Bodélé Depression. Other regions marked are the Hoggar Massif, the Tibesti Massif, and Western Sahara.

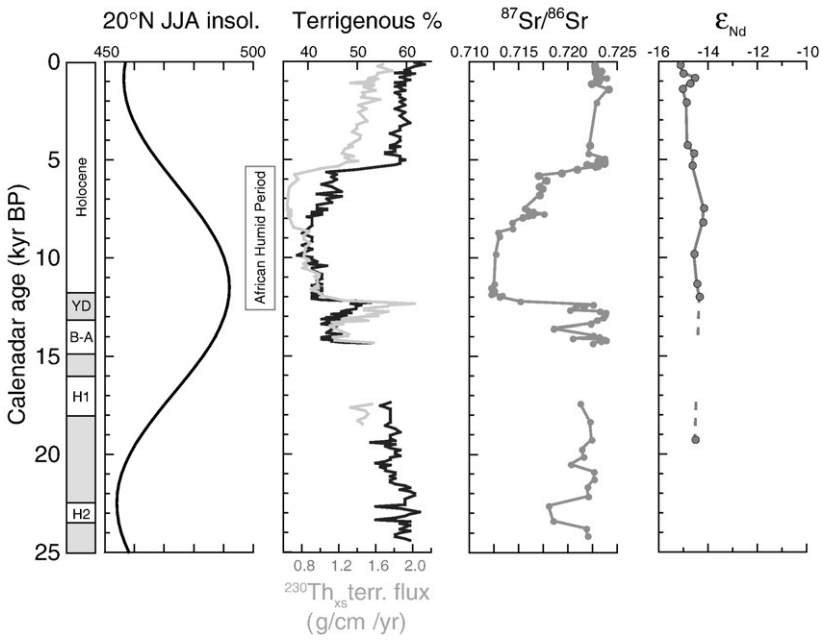

Fig. 2. Changes in sediment composition over time. Age depth model from (deMenocal et al., 2000b), terrigenous percent data from deMenocal et al. (2000a), and $^{230}Th_{xs}$ normalized terrigenous flux data from Adkins et al. (2006). Sr and Nd isotope data from Table 1 of the supplementary material. Large and abrupt changes in the Sr isotope record mirror changes in the percentage and flux of terrigenous material at the site. Nd isotopes remain essentially constant over the record.

equatorial Atlantic into western and central subtropical Africa. Interaction between surface and lower tropospheric disturbances and boreal summer monsoonal circulation establishes fronts of extreme turbulence in the Sahara and northern Sahel, which entrains and lifts mineral dust to mid-tropospheric levels. This dust is transported westward in the Saharan Air Layer and is carried as far west as the Caribbean (Carlson and Prospero, 1972; Prospero and Lamb, 2003; Prospero and Nees, 1986). During boreal winter, the North African landmass cools relative to adjacent ocean and the regional atmospheric circulation reverses; the ITCZ is pushed southward and dry and variable northeast trade winds predominate. A separate dust plume is associated with the NE trade (Harmattan) winds and transports large volumes of dust southwestward, dominantly during winter months (Chiapello et al., 1995).

The northeasterly trade winds establish strong and persistent coastal upwelling along the Northwest African margin (Müller and Fischer, 2001). Currents along the continental rise and margin, including the Canary Current, flowing south along the coast (Mittelstaedt, 1991), and deeper water masses, including the south-flowing North Atlantic Deep Water below ~2000 m and north-flowing Antarctic Bottom water below ~3600 m, facilitate sediment redistribution (Sarnthein et al., 1982).

Satellite imaging of atmospheric aerosols have identified the major dust producing areas of northwestern Africa (Fig. 1) (Prospero et al., 2002). The Bodélé Depression, Chad is the most productive dust source of this region, and on Earth, and other important source areas are the basins east and south of the Ahaggar Mountains (Hoggar Massif), the base of the Tibesti Mountains, and the western coasts of Mauritania and Western Sahara (Prospero et al., 2002). Regions with alluvial and lacustrine deposits are more important dust sources than the course-grained sand seas (Prospero et al., 2002). Some studies have shown that because the Saharan Air Layer occurs at high altitude, winter NE trades deposit much more dust along the eastern margin of the Atlantic Ocean than the summer winds (Chiapello et al., 1997; Chiapello et al., 1995). Stuut et al. (2005) studied the provenance of present-day dust collected in shipboard filters during a transect along Northwest Africa. The sample collected closest to our core showed a dust back-trajectory through Mauritania, Western Sahara, and Algeria. However, this transect was completed during the months of February to March, during the time of year when the NE trade winds dominate, so this study is not representative of SAL summer winds.

2. Materials and methods

Ninety-two 2-cm scrape samples (a 2-cm nylon card was drawn across the width of the core, sampling only ~5 mm of depth but integrating the width) were taken from ODP 658C for isotopic and geochemical analyses. Chemical preparation steps were taken to ensure that these analyses represent the terrestrial component. Samples were wet sieved at 63 μm, oven-dried at ~40 °C, and the fine fraction was gently disaggregated. A sub-sample of the fine fraction (~200 mg) was leached with buffered (with sodium carbonate to pH ~5) acetic acid (HOAc) to remove the calcium carbonate component without altering clays (Biscaye, 1965). Sequential six- to twelve-hour leaches were performed until no bubbles were discerned. One additional HOAc leach was implemented after the last noticeable reaction to ensure all carbonate was removed, and the sample was rinsed three times in deionized water. To remove the authigenic iron (Fe)-manganese (Mn) oxyhydroxide coatings, samples were leached with a hydroxylamine hydrochloride (HH) and 25% HOAc solution for two hours, and then again for six hours (Chester and Hughes, 1967). Samples were then rinsed three times again with deionized water. Samples were not leached for opal or organic carbon. deMenocal et al. (2000a) reported that biogenic opal concentration reached a maximum of 8% in this core, and low organic carbon contents between 0.5 and 1.5%. Due to the low concentration of Sr and Nd in biogenic opal, this fraction would have negligible effect on the radiogenic isotope ratios (Bayon et al., 2002), but some of the observed variations in major and trace element chemistry may result from contributions by the opal component.

The remaining siliciclastic sample was processed for Sr and Nd isotope and major and trace element measurements. For Sr and Nd isotope analysis, samples were dissolved in Savillex vials in a mixture of nitric acid (HNO_3)-hydrofluoric acid (HF)-perchloric acid ($HClO_4$). Samples for Sr analyses were purified on 30 μL Teflon columns filled with Eichrom Sr-spec resin in 3 N HNO_3. Nd cuts were purified first

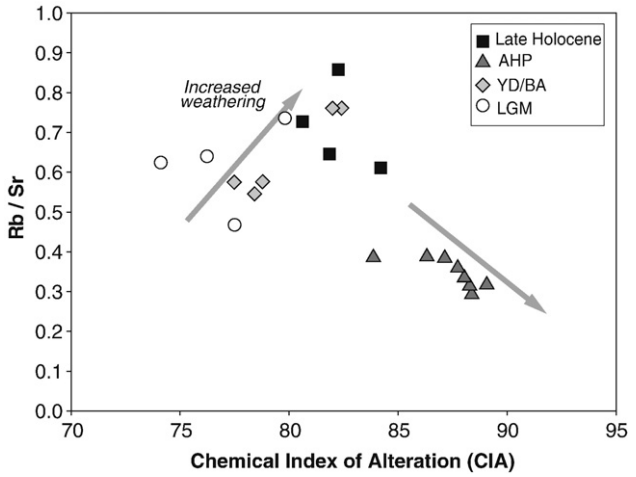

Fig. 3. Rb–Sr ratios versus the Chemical Index of Alteration (CIA). Rb/Sr is expected to increase with increased weathering, due to the association of Rb with mica-rich clays. CIA is a measure of weathering using the mole fractions of the oxides of Al, Ca of the silicate fraction, Na, and K. Samples from the LGM, Younger Dryas/Bølling-Allerød, and late Holocene all plot along the expected weathering trend. Samples from the African Humid Period however form their own array with decreased Rb/Sr and increased CIA (Table 2 of the supplementary material).

using100 µL Teflon columns with Eichrom TRU-spec resin in 1.6 N HNO_3 to separate the rare earth elements (REE) from other cations and then in 800 µL Savillex columns with Bio-Rad AG50W-X4 resin in alpha-hydroxyisobutyric acid (α-HIBA) to isolate the Nd.

All isotopic measurements were made on a VG Sector 54-30 thermal ionization mass spectrometer at Lamont–Doherty Earth Observatory. Sr samples were loaded on tungsten (W) filaments with a tantalum chloride (TaCl) solution (Birck, 1986) and measured in multidynamic mode. $^{87}Sr/^{86}Sr$ ratios were normalized to $^{86}Sr/^{88}Sr=0.1194$. Replicate measurements of SRM (standard reference material) 987 resulted in an average $^{87}Sr/^{86}Sr=0.710256$, 2σ external reproducibility of ±0.000023 ($n=26$), and samples were corrected to a value of 0.710245. Nd isotopes were measured on rhenium (Re) filaments in oxide form using either an oxygen (O) leak valve or loading in colloidal silica gel as the source of O_2. $^{143}Nd/^{144}Nd$ ratios were normalized to $^{146}Nd/^{144}Nd=0.7219$. Multiple measurements of the La Jolla Nd standard averaged $^{143}Nd/^{144}Nd=0.511851$, 2σ external reproducibility of ±0.000024 ($n=13$), and ratios were corrected to a value of 0.511860. Sr isotopes are reported for 92 samples spanning the last ~25 kyr from ODP 658C, with sample spacing between 2 and 28 cm (~50 to ~2200 years). The hiatus from 17.2 ka to 14.8 ka (deMenocal et al., 2000b) precluded sampling of the interval between the LGM and the Bølling-Allerød. Nd isotope ratios are reported for 12 samples.

Twenty-one processed (sieved, decarbonated, Fe–Mn leached) samples were also analyzed for major and trace elements by inductively couple plasma mass spectrometry (ICP-MS) and inductively coupled plasma emission spectrometry (ICP-ES) at Boston University. Samples were dissolved by microwave digestion in an HNO_3-HF-hydrochloric acid (HCl)-hydrogen peroxide (H_2O_2)-boric acid (H_3BO_3) mixture. Methods are based on published procedures (Kelley et al., 2003; Murray et al., 2000). Digestion blanks were generally less than 3% of an average sample. Analytical precision was between 3% and 5%.

To aid in the interpretation of the major element geochemistry, we calculated the chemical index of alteration (CIA), which is the molecular proportions of the oxides of aluminum (Al), calcium (Ca) of the silicate fraction, sodium (Na), and potassium (K) through the formula (McLennan, 1993; McLennan et al., 1993; Nesbitt and Young, 1984):

$$CIA = \left(\frac{Al_2O_3}{Al_2O_3 \times CaO_{(sil)} \times Na_2O \times K_2O}\right) \times 100$$

CIA estimates the extent of weathering continental rocks and sediments, where higher values indicate greater alteration, and has been shown to be very useful in the interpretation of marine sediments (e.g., Colin et al., 2006; Eisenhauer et al., 1999; Hemming, 2007; McLennan et al., 1990).

3. Results

$^{87}Sr/^{86}Sr$ ratios show a large variation (~0.714 to ~0.723) and the pattern strongly resembles variations in percent terrigenous material and $^{230}Th_{xs}$ normalized terrigenous flux (Fig. 2, Table 1 of the supplementary material). The oldest data from the LGM show high $^{87}Sr/^{86}Sr$ ratios of ~0.722. Values remain generally high, between ~0.721–0.722, to ~14.5 ka. Two samples at ~24–22 ka are lower than average LGM values with $^{87}Sr/^{86}Sr=0.7185$, and may correspond to Heinrich event H2 (23.4–22.6 ka in the Site 658C age model (deMenocal et al., 2000a; deMenocal et al., 2000b). There is a hiatus from 17.4 to 14.8 ka. Most of the 18 samples over the interval of ~14.2 to 12.4 ka, corresponding to the Bølling–Allerød to Younger Dryas, show largely the same range as the LGM, but include a few samples with lower values to ~0.718. Following a

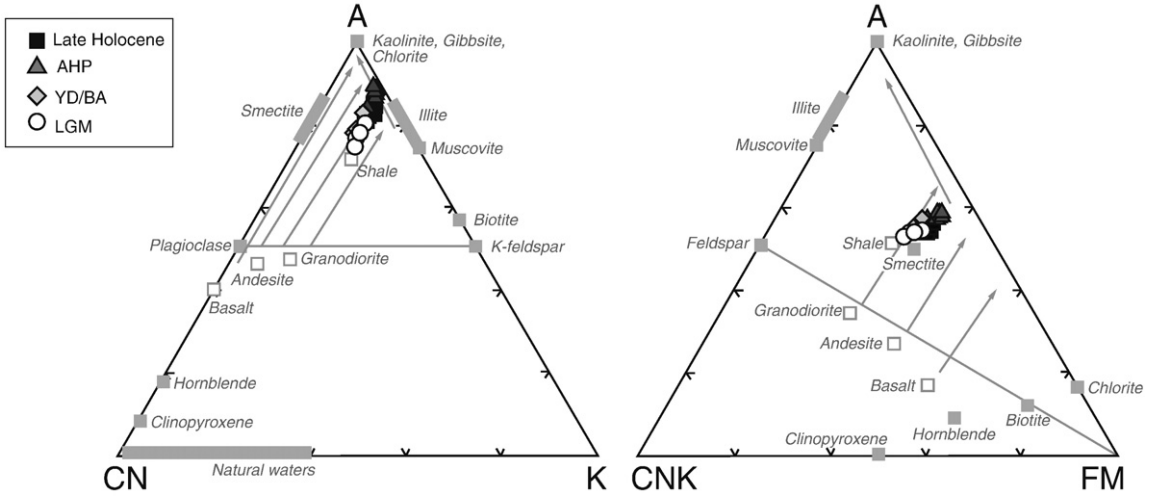

Fig. 4. Ternary diagrams of data from Table 2 of the supplementary material, plotted using program of John (2004). Abbreviations for the apices are, in mole fraction: $A=Al_2O_3$, C = CaO of the silicate fraction, $N=Na_2O$, $K=K_2O$, $F=Fe_2O_3$ total, and M = MgO. Simplified compositions for minerals, rock types, and natural waters are shown for comparison and arrows represent general weathering trends (McLennan et al., 1993). Samples from ODP 658C fall along these general trends, with AHP samples the most evolved.

peak within the Younger Dryas (~12.5 ka) a large and abrupt transition then occurs over ~5 cm or ~150 years to much lower $^{87}Sr/^{86}Sr$ ratios of ~0.716 to 0.714. For the next ~6 kyr, $^{87}Sr/^{86}Sr$ remains low, forming the most distinctive aspect of the time series data. Commencing at ~8.7 ka samples show a gradual increase to ~0.718 at ~6 ka, although within this interval there is a brief excursion to lower values near 8 ka. Another abrupt transition occurs at the termination of the AHP, with $^{87}Sr/^{86}Sr$ increasing back to LGM- and Bølling–Allerød-type values of ~0.722 by 5.4 ka. From then to the present day, Sr isotopes remain between 0.721 and 0.723, showing little variation. Detailed analyses were conducted spanning the last 1000 years to capture the Little Ice Age–Medieval Climate Anomaly oscillation; no significant compositional variability was observed over this period.

Nd isotopes on a more limited set of samples show little variation even across the most profound changes in Sr isotope data (Fig. 2, Table 1 of the supplementary material). Samples from ODP 658C have average ε_{Nd} (the deviation in parts per 10,000 of the measured $^{143}Nd/^{144}Nd$ ratio from the chondritic uniform reservoir or "CHUR" value of 0.512638 (Jacobsen and Wasserburg, 1980), representing the average Earth) of about −14.6 and a total range from −14.2 to −15.1, corresponding to an average depleted mantle Nd model age of ~1.9–2 Ga (c.f. Goldstein et al., 1984; Taylor et al., 1983).

To better constrain the processes controlling terrigenous sediment compositions at ODP Site 658C, we selected 21 samples for major and trace element analyses (Table 2 of the supplementary material). Our analyses differ from the study by Haslett and Davies (2006) on the same core, as we have focused on the terrigenous component (by dissolving biogenic carbonate) and have measured a larger number of elements. We divide our samples into four time periods: four (from 20–119 cm) are late Holocene, eight (from 131–257 cm) are from the AHP, four (262–324 cm) are from the Younger Dryas/Bølling–Allerød, and four (339–420 cm) are LGM. Major elements are a useful determinant of degrees of weathering in bulk sediments. ODP 658C samples show a range of CIA values between 74 and 89 (Fig. 3, Table 2 of the supplementary material). On ternary diagrams they lie on well-defined chemical weathering trends from the composition of "average shale", represented by Post-Archean Australian Shale (PAAS) (Taylor and McLennan, 1985) to more highly weathered compositions (Fig. 4). The AHP samples show the highest weathering index values, with CIA ≥84. The higher CIA is reflected in enrichment of Al, Mg, and Si compared to Ca and Na.

Whereas the high CIA values imply high Al compared to soluble elements, AHP sample also show high abundances of Sr. On a classical linear mixing diagram plotting Sr isotopes vs. 1/Sr (Fig. 5), it can be clearly

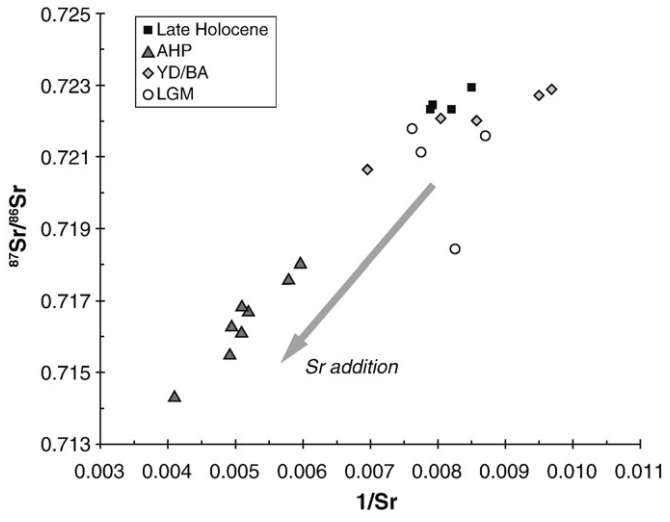

Fig. 5. $^{87}Sr/^{86}Sr$ against 1/Sr. This plot demonstrates that the African Humid Period samples are greatly enriched in Sr relative to samples from arid periods (Tables 1 and 2 of the supplementary material).

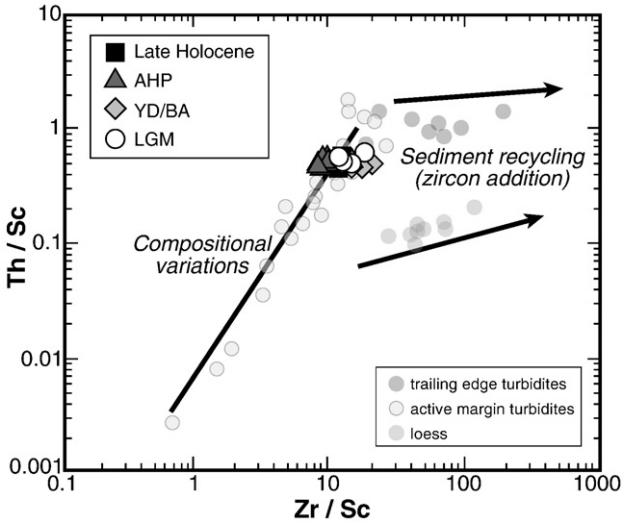

Fig. 6. Th/Sc versus Zr/Sc after McLennan et al. (1993). This plot distinguishes compositional variations from those due to sedimentary sorting and recycling. All samples have roughly equal Th/Sc, indicating similar provenance. Samples from the AHP have the lowest Zr/Sc, while Younger Dryas, Bølling-Allerød, and LGM samples have the highest Zr/Sc. High Zr/Sc is indicative of heavy mineral enrichment. Turbidite data from McLennan et al. (1990) and loess data from McLennan (2001).

seen that low $^{87}Sr/^{86}Sr$ reflects addition of a Sr-rich component, especially in the AHP samples. Moreover, this component has low rubidium (Rb)/Sr (Fig. 3). Thorium (Th)–scandium (Sc) ratios are relatively constant among all ODP 658C samples, while zirconium (Zr)–Sc ratios are generally lower in AHP (Fig. 6, Table 2 of the supplementary material). Similarly, titanium (Ti)–(Al) ratios are lower in the AHP compared to other times (Table 2 of the supplementary material). All samples show varying degrees of low REE compared to PAAS, but maintain the general trend of light REE enrichment, negative europium (Eu) anomalies, and flat heavy REE (Table 2 of the supplementary material). Given the strong association between barium (Ba), opal, and organic matter (e.g. Bishop, 1988), Ba concentrations (Table 2 of the supplementary material) were compared to opal percentages (deMenocal et al., 2000a). No correlation exists between these two variables, indicating that the small amount of opal present in our samples does not significantly contribute to the bulk geochemical patterns.

4. Discussion

The ODP 658C data document sudden and large magnitude changes in the $^{87}Sr/^{86}Sr$ of the terrigenous input over the past 25 kyr (Fig. 2). Variations in major and trace element chemistry suggest changes in sedimentary processes or sources through time. Together, these data can be used to assess the relative influences of four possible mechanisms: (1) changes in the source terranes, (2) changes in the degree of chemical weathering of the same source terrane, (3) physical sorting of minerals derived from the same sources, e.g., wind versus river or stronger versus weaker winds, and (4) variability in contributions from different possible sources within a terrane.

4.1. Evidence for constant sedimentary provenance terrane type and age

The nearly invariant Nd isotope and Th–Sc ratios suggest a constant geologic source terrane for the terrigenous supply to ODP 658C over the last 25 kyr. Samarium (Sm)–Nd ratios of continental sediments show only a small range, nearly 40% lower than the bulk Earth (Goldstein et al., 1984; Taylor et al., 1983), and Sm and Nd are both resistant to weathering. As a result, Nd isotope ratios effectively represent the average "crustal residence age" of the continental sediment sources, which in our case is ~1.9–2.0 Ga. The complex geologic history of the African continent yields a wide range in ε_{Nd} of potential source

materials, from about −12 to −18 (Grousset et al., 1998). The nearly constant Nd isotope ratios throughout our 25 kyr record strongly indicate that the age of the continental basement sources of the material did not change (Fig. 2). The average ε_{Nd} for the entire record is −14.6, and while there appears to be a slight difference between the late Holocene (average −14.8, $n=9$) and the AHP (average −14.3, $n=5$), it is within the external 2σ uncertainty (approximately ±0.5 epsilon units) and may be related to small number of samples.

Our ODP Site 658 data are consistent with those of Grousset et al. (1998), who analyzed Holocene-LGM sample pairs off the coast of West Africa between 0° and 34°N. Although they found lower LGM values (ε_{Nd} of −16 to −19) in shallow cores (<1500 m depth) along the African shelf closest to our sampling site, in deeper cores (>3000 m depth) west of the continental margin they found similar Holocene-LGM ε_{Nd} values to ours (around −13 to −14). This may indicate that the shallow cores in the Grousset et al. (1998) study source a different region than their deeper cores, and ODP Site 658. More recently, Jullien et al. (2007) collected downcore Sr and Nd isotope ratios from a core (MD03-2705) located just southwest of ODP 658C. Analyses were collected for samples that corresponded to either the height of a low-latitude "dusty" event or so-called "glacial background," and the AHP was not captured in this study. Nd isotope ratios do not vary greatly (ε_{Nd} from −14.0 to −15.4) and the Younger Dryas ε_{Nd} is −14.6 (Jullien et al., 2007), corresponding precisely with the average from ODP 658C.

Trace element ratios can provide another indicator of provenance. For example, Th and Zr behave incompatibly in igneous processes, while Sc is compatible, but Zr can be enriched in sediments due to heavy mineral (zircon) sorting (Hemming, 2007; McLennan et al., 1993; Taylor and McLennan, 1985). As expected, all samples from ODP Site 658C all show similar Th/Sc (Fig. 6), indicating the same general provenance.

4.2. Geochemical and isotopic perspectives on weathering

While sediments from the AHP in ODP 658C show certain highly weathered characteristics, such as high CIA (Fig. 3, 4) and high lithium (Li) concentrations (Table 2 of the supplementary material), other qualities contradict expectations with increased weathering, such as low Rb/Sr and high Sr and magnesium (Mg) concentrations (Fig. 3, 5, Table 2 of the supplementary material).

Rb/Sr of continental rocks vary greatly and can be modified by weathering and mineral sorting. For example, high Rb/Sr in mica impart high Sr isotope ratios over time, while Sr isotope ratios of plagioclase or calcite do not change very much due to their low Rb/Sr. Thus sediment samples from the same source terrane can show very large differences in Sr isotope ratios. Recent studies found large temporal shifts in the Sr isotope ratios of marine sediments, and attribute them to changes in the degree of physical versus chemical weathering on land (Colin et al., 2006; Jung et al., 2004). The response of Rb–Sr isotopes to chemical weathering is complex and reflects the aqueous geochemistry of fluid-rock interactions (Blum and Erel, 1997; Blum et al., 1993; Bullen et al., 1997; Dasch, 1969), where Sr behaves like Ca, and is liberated to the fluid, while Rb is analogous to K, and tends to stay with the residue. During continental weathering, phases such as plagioclase (bearing Ca and Sr) break down early on and release labile elements. Because plagioclase has low Rb/Sr, the released Sr has low $^{87}Sr/^{86}Sr$, leaving a residue with higher $^{87}Sr/^{86}Sr$. On the other hand, rivers and streams sometimes have higher $^{87}Sr/^{86}Sr$ than the rocks they weather (Blum and Erel, 1997; Blum et al., 1993; Bullen et al., 1997). This has been attributed to the preferential leaching of radiogenic ^{87}Sr, which fits poorly in the damaged lattice site that contained Rb at the time of crystallization. The breakdown of Rb-rich micas early in the weathering sequence releases radiogenic Sr to the fluid. In all these cases, Rb and K are retained in the relict "incongruently weathered" material, increasing its Rb/Sr. Studies of weathering profiles show that the increase in the Sr isotope ratios is a function of age, Rb enrichment, and reactivity of the mineral assemblage (Dasch, 1969). Therefore the expectation is that Rb/Sr generally increases in the residue with increasing degrees of chemical weathering (Hemming, 2007), due to loss of soluble Sr and/or addition of Rb, and with sufficient elapsed time, the higher Rb/Sr further generates high $^{87}Sr/^{86}Sr$ ratios in the weathered material.

A recent study of a marine sediment core in the Arabian Sea over the last 10 kyr by Jung et al. (2004) proposed that Sr isotope variations reflect the relative importance of physical versus chemical weathering of terrestrial sediments in northeast Africa. Nd isotopes show limited variability, slightly increasing in the older part of the record from ε_{Nd} of approximately −6.6 at 9.6 ka to −5 at 8.5 ka. In contrast, Sr isotopes exhibit large shifts. The lowest values are observed during the AHP ($^{87}Sr/^{86}Sr=\sim0.7137$) between ~10 to 8.5 ka, when there is an abrupt increase to ~0.714–0.715. At ~6.5 ka the Sr isotope ratios begin to gradually increase again, reaching the highest values ($^{87}Sr/^{86}Sr=\sim0.7168$) between 2 ka and today. Jung et al. (2004) suggest that low Sr isotopes in sediments reflect domination by chemical weathering associated with increased monsoonal precipitation and leading to loss of high Rb/Sr phases (e.g., mica and K-feldspar) and radiogenic Sr from the terrigenous detritus source. Conversely, they interpret high Sr isotopes to reflect domination by physical weathering and preservation of high Rb/Sr phases during arid intervals. Another study by Colin et al. (2006), of marine sediments from the Bay of Bengal and the Andaman Sea, also find glacial–interglacial changes in Sr isotopes, with higher values in glacial sediments, which they attribute to efficient transport of high K minerals released by glacial scouring in the Himalayas, and lower Sr isotope ratios during interglacials when scouring and transport is not as efficient, chemical weathering is more intense, and radiogenic Sr has been lost to the fluid.

The CIA (c.f. McLennan, 1993; McLennan et al., 1993; Nesbitt and Young, 1984) is a useful measure of weathering in sediments. The CIA of average upper continental crust is about 47 and values between 45 and 55 indicate the absence of extensive chemical weathering. Removal of alkalis and alkaline earths through intense chemical weathering can cause CIA values to approach 100. ODP Site 658C samples show a range of CIA values between 74 and 89 (Fig. 3), corresponding values for average shale to more highly weathered compositions. The AHP samples show the highest CIA with values ≥84 (Table 2 of the supplementary material). Thus the high CIA values are consistent with increased chemical weathering to residual Al-rich clay minerals, and consistent with increased precipitation and chemical weathering associated with the AHP. When plotted on ternary diagrams, our samples fall along expected weathering trends, with AHP samples the farthest along on these trends (Fig. 4). Others have shown that Li tends to increase with increasing CIA in shales (Teng et al., 2004), and we observe high Li concentrations with the higher CIA values of the AHP.

In ODP 658C, Sr isotope ratios and major and trace element concentrations appear to give conflicting results concerning the indicators of chemical weathering. Like the Arabian Sea data, Sr isotopes are lower in ODP 658C sediments during the AHP (Fig. 2), when precipitation was higher. However, Rb/Sr is also lower in AHP samples (Fig. 3), which is opposite of the expectation of increasing Rb/Sr with increasing weathering. AHP samples are associated with significantly increased Sr concentrations (Fig. 5, Table 2 of the supplementary material), demonstrating an addition of Sr to these samples, which is surprising given CIA values that show AHP samples have lost other labile elements like Ca and Na. Mg is also enriched in AHP sample, behaving similarly to Sr and counter to the expectation of loss with increased weathering. Large ion lithophile elements like Rb and Ba are low in AHP samples, however, smaller Li is moderately enriched. Consequently, a simple increase in chemical weathering of sediments from a constant source during the AHP does not explain our data.

4.3. Evaluation of size sorting indicators

Variations in ODP 658C samples are also not easily interpreted a resulting from grain-size sorting. African Humid Period samples have

high CIA and low Zr/Sc and Ti/Al typical of fine fraction sediments, but also have low Sr isotope and Rb–Sr ratios expected in coarser sediments.

In a new study, Tjallingii et al. (2008) present grain-size data on siliciclastic sediments from a marine core (GeoB7920) located very close to ODP Site 658C. Grain-size distributions were divided into three end members, with dominant modal grain-sizes of 57.8 μm (EM1), 34.6 μm (EM2), and 4.9 μm (EM3). EM1 and EM2 are interpreted to be aeolian in origin, while EM3 is thought to be derived from riverine inputs. During the AHP, EM3 provides the greatest contribution. Additionally, a large submarine canyon has been recently identified to the south of ODP Site 658C (Krastel et al., 2004). It is thought this canyon was formed in relation to an ancient river system, and it has been suggested that the channel system may have been active in the early Holocene (Zühlsdorff et al., 2007), perhaps providing some of the EM3 material found in the GeoB7920 core (Tjallingii et al., 2008).

Based on the Tjallingii et al. (2008) results, one might expect ODP 658C sediments from the AHP to be dominated by a fluvially derived fine fraction. The depletion of the ODP 658C core prevented sampling enough material to collect traditional grain-size analysis data. However, major and trace element geochemistry can help to decipher sedimentary sorting and recycling (McLennan et al., 1993). Silicon (Si)-Al ratios can represent the proportions of quartz to clays, and therefore are expected to decrease with decreasing grain-size. Physical sorting changes Zr/Sc and Ti/Al, as Zr and Ti indicate the presence of heavy minerals such as zircon, rutile, and ilmenite, while Sc and Al are enriched in clays rather than heavy accessory phases. Hafnium (Hf) concentrations are also expected to be higher due to the abundance of Hf in zircons. Rb/Sr also can be changed by sedimentary sorting, tending toward increased Rb/Sr with decreasing particle size, since more mica-rich clay fraction have high Rb/Sr, and coarser feldspar-rich sediments have low Rb/Sr (Hemming, 2007). Therefore, an effect of sorting on the fine grain size fraction would show increased CIA and mature clay mineralogy, high Rb/Sr, and low Si/Al, Zr/Sc, Ti/Al, and Hf reflecting high clay relative to heavy mineral abundances.

Other studies have demonstrated a relationship between Sr isotope ratios and grain-size (c.f. Biscaye and Dasch, 1971; Dasch, 1969; Walter et al., 2000). Most of the samples analyzed from those studies show that $^{87}Sr/^{86}Sr$ increases with decreasing grain-size. Jung et al. (2004) also demonstrated higher $^{87}Sr/^{86}Sr$ on the less than 2 μm compared to the less than 63 μm size fractions for six samples from their Arabian Sea sediments. The strong co-variation between the Sr isotope ratios for the two size fractions for each sample, suggesting that in this location at least, the two size fractions have the same source (Jung et al., 2004). This pattern of high Sr isotope ratios with decreasing grain-size is an extension of the high Rb/Sr in finer (mica-rich) sediments, as the decay of ^{87}Rb results in ^{87}Sr.

Other studies have shown that Nd isotope ratios are unaffected by grain-size variations (Goldstein et al., 1984; Grousset et al., 1992). However, it might be expected that sediments transported by riverine versus aeolian processes could have different ultimate sources and therefore different Nd isotope ratios.

In ODP 658C samples, we observe high CIA, low Zr/Sc, Ti/Al, and Hf during the wet AHP, all consistent decreasing grain-size relative to the drier Younger Dryas and LGM (Fig. 3, Table 2 of the supplementary material). Si/Al does not vary greatly in these samples, but is indeed moderately lower during the AHP (Table 2 of the supplementary material). The lack of variability in Nd isotopes implies a consistent geologic source terrane, and may indicate that changes in process based sorting (i.e. aeolian versus fluvial) did not occur over the record. Furthermore, in AHP samples, $^{87}Sr/^{86}Sr$ values are the lowest and we see a decrease in Rb/Sr associated with increased Sr concentrations (Fig. 2, 3, 5). The large and abrupt decrease in $^{87}Sr/^{86}Sr$ during the wettest period is a strong argument against grain-size variations as an explanation for the ODP 658C siliciclastic sediments.

4.4. Evidence for variability in contributions from different sources within a terrane

The ODP 658C Nd isotopic data indicate no significant changes in geologic source terrane, and the geochemical data are ambiguous regarding implications for variations in weathering régimes or physical sorting. We propose that the compositional changes associated with the AHP interval indicate an additional, authigenic mineral component associated with paleolake basins that were prevalent across North Africa at this time. This authigenic component is characterized by its highly weathered composition (high CIA) and fine particle size (based on low Si/Al, Zr/Sc, Ti/Al, Hf; and grain-size evidence from Tjallingii et al. (2008)), but it is also enriched in some labile elements (high Sr, Mg, and low Rb/Sr, which are consistent with a precipitated phase) and has the lowest $^{87}Sr/^{86}Sr$ observed in the record (Figs. 2–6, Table 2 of the supplementary material).

This component may have formed in association with lakes, which were more numerous and widespread during the AHP. Seasonal desiccation of these lake basins may have presented important additional sources of mineral dust. Combined with a lower overall aeolian flux, such a dust source could have a significant impact on the Sr isotope record during the AHP. In this scenario, the $^{87}Sr/^{86}Sr$ of the authigenic end member would simply reflect the $^{87}Sr/^{86}Sr$ of the water, as would the ε_{Nd} of that end member. Both could very well represent the average composition of the local drainage basin, particularly if there are carbonate or evaporite deposits having high Sr and low $^{87}Sr/^{86}Sr$, but also having the low Nd and ε_{Nd} matching the surrounding terranes. This component would have precipitated from the lake waters, likely saline and alkaline, and the low Rb/Sr and high Sr and Mg concentrations reflect the availability of these ions in water (Figs. 3, 4, 5). Phosphorus (P) is also high during the AHP, with concentrations greater than can be accounted for by apatite with respect to CaO, and may reflect increased organic material that could be associated with lakes as well. As this new component is enriched in both Al and Mg (Fig. 4, Table 2 of the supplementary material), it may contain phases like the Mg-rich clay palygorskite, which can be found in arid lacustrine deposits (Tateo et al., 2000). Freshwater diatoms from lacustrine sources have been previously found in marine sediments off Northwest Africa, so it may be possible to further document a lacustrine source in AHP sediments (e.g., Gasse et al., 1989).

In this context, a recent study by Moreno et al. (2006) has shown that modern dust collected in the Bodélé Depression of the Chad Basin has relatively high CIA and low Rb/Sr and Zr/Sc ratios, very similar to the composition of our AHP samples. That study did not measure Sr isotopes on those sediments, but our interpretation would be tested by such measurements as our prediction is that their isotope composition would be close to that of our AHP samples. Our interpretation is also consistent with the Nd isotope data. Because Nd isotopes tend to be the same in samples that have undergone different stages of weathering, we would expect the isotopic composition of the lake water to be the same as the surrounding terranes and thus the local terrigenous sediments.

We can provide a rough estimate of the time-varying contribution of this hypothesized authigenic component. The $^{230}Th_{xs}$ derived sediment flux estimates document that total terrigenous supply decreased during the AHP to less than half the LGM and late Holocene rates (Fig. 2) (Adkins et al., 2006). Therefore, mass balance does not require a large flux of this authigenic component to affect the Sr isotopic composition of the sediments. We used the measured Al/(Ca+Na) ratio to represent the degree of alteration. Samples with the lowest Al/(Ca+Na) ratios plot near average shale on the CIA ternary diagram, while samples with the highest Al/(Ca+Na) ratios plot near the edge (Fig. 4). Using the linear correlation between measured $Al_2O_3/(CaO+Na_2O)$ and Sr isotope ratios in the limited samples with both measurements, we estimate alteration index of samples where we have Sr isotopes but no major element data. The exclusion of two outliers yields a high correlation coefficient. The

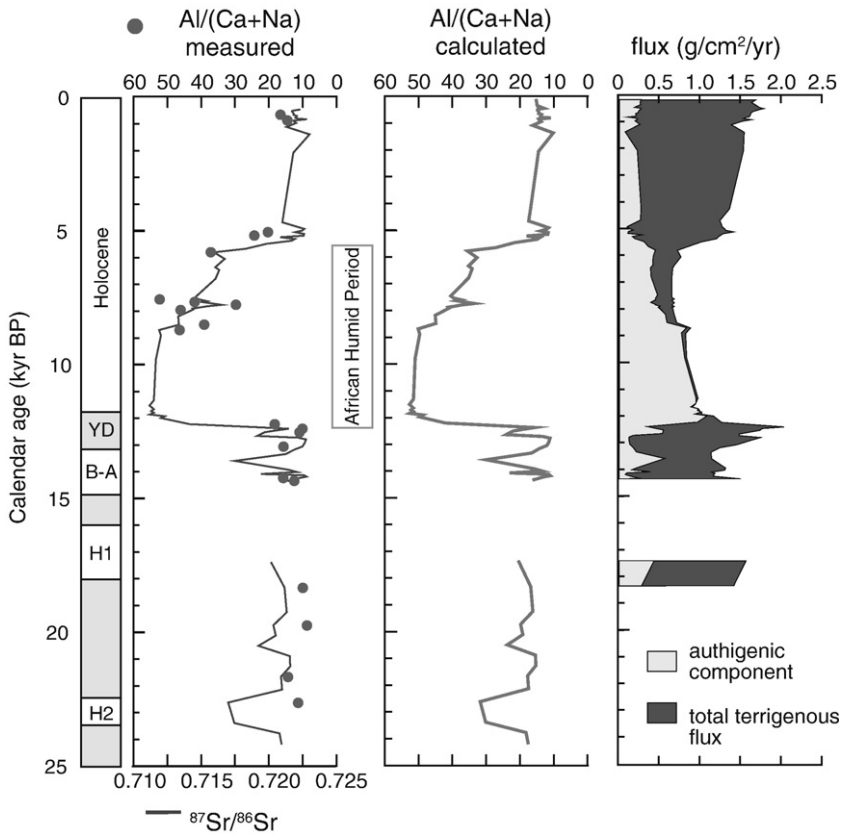

Fig. 7. Measured $Al_2O_3/(CaO+Na_2O)$ and $^{87}Sr/^{86}Sr$ are plotted against age. A linear regression between $^{87}Sr/^{86}Sr$ and $Al_2O_3/(CaO+Na_2O)$ (excluding samples from 257 and 420 cm depth) resulted in the equation $y=-4462\times{}^{87}Sr/^{86}Sr+3237$ with an $R^2=0.78$. The relationship was used to calculate $Al_2O_3/(CaO+Na_2O)$ for all samples with a Sr isotope measurement. Then two extremes were determined, the highest $Al_2O_3/(CaO+Na_2O)$ representing one extreme, and average shale representing the other. From this two-component mix, we calculated the proportion of the shale-like end member to the end member with the largest authigenic component through time. The $^{230}Th_{xs}$ normalized terrigenous flux (Adkins et al., 2006) was then multiplied by the fraction of the authigenic end member to calculate its flux over time, and compared to total terrigenous flux. This graph shows that the authigenic end member dominated in the AHP, when the overall terrigenous flux is the lowest.

calculated CIA values are given in Table 3 of the supplementary material. We then set average shale as the unaltered endmember and the sample with the highest $Al_2O_3/(CaO+Na_2O)$ ratio (248 cm) as the authigenic aluminosilicate end member and calculated the fraction of the AHP component in each sample. This fraction was then multiplied by the ^{230}Th normalized terrigenous flux to calculate the flux of the new material over time (Fig. 7, Table 3 of the supplementary material).

This calculation allows us to estimate the time-varying contribution of the authigenic component to the overall terrigenous sediment flux record. We do not propose that the sample at 248 cm is a pure example of the authigenic component, but this method of calculation provides an upper limit to the flux volume attributable to the authigenic component over the last 25 kyr. The greatest flux of this proposed authigenic component occurred between 12.3 and 8.2 ka, and this component dominates the terrigenous supply until the end of the African Humid Period near 5.5 ka, after which the terrigenous chemistry shifts abruptly and completely to the relatively unaltered shale-like background dust.

4.5. Perspective on the nature of the termination of the AHP

These new results from ODP 658C bolster the case for an abrupt termination of the AHP in northwestern Africa. Our high-resolution $^{87}Sr/^{86}Sr$ record demonstrates an abrupt shift to high values over the period of a few hundred years near 5.5 ka (Fig. 2). Geochemical data indicate that not only did the Saharan aeolian flux dramatically increase after 5.5 ka, reflecting the abrupt onset of hyperarid conditions; but if the interpretation of a lacustrine contribution during the AHP holds, the transition to higher $^{87}Sr/^{86}Sr$ at ca. 5.5 ka may document terminal desiccation and deflation of paleolake basin sediments (Figs. 2, 7). Organic molecular plant wax biomarker data from ODP 658C document vegetation changes that were synchronous with the dust flux and terrigenous geochemistry changes reported here, and they were equally abrupt (Zhao et al., 2003). Published results from Lake Bosumtwi and other Northwest African lake basins have also proposed rapid (century-scale) transitions from the wetter conditions of the AHP to the arid conditions of the late Holocene, although the mid-Holocene timing of this transition varies regionally (Gasse, 2000; Gasse et al., 1990; Gasse and Van Campo, 1994; Russell et al., 2003). These results differ appreciably from the more gradual, millennial-scale AHP termination reported from Lake Yoa in the hyperarid Saharan desert sector of northern Chad (Kröpelin et al., 2008). Fossil pollen preserved in this unique, groundwater-fed lake basin indicates a gradual transition from tropical wooded grasslands to desert flora between 4.3–2.7 ka. Diatom and chironomid-inferred changes in lake conductivity, however, do reveal the very abrupt (century-scale) increase in lake paleosalinity after 4.0 ka when the lake shifted from fresh to hypersaline conditions. An isotopic study of Arabian Sea sediments also documents a more gradual termination of the AHP in the eastern Sahara (Jung et al., 2004). Collectively, these results depict a dynamic, time-transgressive evolution of North African paleoclimate change during the mid-Holocene.

5. Conclusions

This study used isotopic and chemical analyses of the siliciclastic terrigenous fraction deposited in the eastern Atlantic near the Sahara at ODP Site 658C over the last ~25 kyr to trace the history of those

sediments over the LGM and the Holocene, when the climate was arid, and through the African Humid Period. Nd isotope ratios show little variability throughout the interval, indicating that the contributing geological terranes have not changed. However, there are major differences in the Sr isotope ratios and sediment chemistry during the African Humid Period compared to the arid intervals before and after. The AHP samples have attributes that indicate a weathered composition, including higher CIA, compared to the late Holocene and the LGM. Also, these samples have characteristics often associated with fine grain-size, such as high CIA and low Zr/Sc and Ti/Al. However, low Sr isotope ratios, high Sr and Mg concentrations, and low Rb/Sr oppose the expectation for both weathered and fine fraction materials. One intriguing explanation for these date is the addition of an apparently authigenic phase, which is enriched in soluble elements like Sr and formed in ephemeral lakes, to the weathered substrate. More work, such as X-ray diffraction analysis, would be needed to specifically identify the phase(s) present in ODP 658C.

Acknowledgements

We thank the Ocean Drilling Program for sediment samples. This work was partially supported by an Earth Institute Postdoctoral Fellowship and an LDEO Climate Center grant (JMC), a grants/cooperative agreement (CICAR) from the National Oceanic and Atmospheric Administration (SRH and SLG), LDEO start-up funds (SLG), NSF awards OCE-04-02348 and HOMINID BCS-02-18511 to (PBdM), and funding from Gary Comer Science and Education Foundation (SRH). The views expressed herein are those of the authors and do not necessarily reflect the views of NOAA or any of its sub-agencies. We thank Louise Bolge and Rick Murray of Boston University for ICP-AES and ICP-MS analyses. We are grateful to Patty Catanzaro for drafting assistance. We thank Sean Higgins and Pierre Biscaye for fruitful discussions, and Jan-Berend Stuut, Mike Krom, one anonymous reviewer, and Editor Peggy Delaney for comments that greatly improved this manuscript. This is Lamont-Doherty Earth Observatory Contribution 7229.

Appendix A. Supplementary data

Supplementary data associated with this article can be found, in the online version, at doi:10.1016/j.epsl.2008.12.011.

References

Adkins, J., deMenocal, P., Eshel, G., 2006. The “African Humid Period” and the record of marine upwelling from excess 230Th in Ocean Drilling Program Hole 658C. Paleoceanography 21, PA4203. doi:10.1029/2005PA001200.

Ahmad, S.M., Babu, G.A., Padmakumari, V.M., Dayal, A.M., Sukhija, B.S., Nagabhushanam, P., 2005. Sr, Nd isotopic evidence of terrigenous flux variations in the Bay of Bengal: implications of monsoons during the last ~34,000 years. Geophys. Res. Lett. 32, L22711. doi:10.1029/2005GL024519.

Bacon, M.P., 1984. Glacial to interglacial changes in carbonate and clay sedimentation in the Atlantic Ocean estimated from 230Th measurements. Isot. Geosci. 2, 97- 11.

Bayon, G., German, C.R., Boella, R.M., Milton, J.A., Taylor, R.N., Nesbitt, R.W., 2002. An improved method for extracting marine sediment fractions and its application to Sr and Nd isotopic analysis. Chem. Geol. 187, 179–199.

Birck, J.L., 1986. Precision K–Rb–Sr isotopic analysis: application to Rb–Sr chronology. Chem. Geol. 56, 73–83.

Biscaye, P.E., 1965. Mineralogy and sedimentation of recent deep-sea clay in the Atlantic Ocean and adjacent seas and oceans. Geol. Soc. Am. Bull. 76, 803–832.

Biscaye, P.E., Dasch, E.J., 1971. The rubidium, strontium, strontium isotope system in deep-sea sediments: Argentine Basin. J. Geophys. Res. 76, 5087–5096.

Bishop, J.K.B., 1988. The barite-opal-organic carbon association in oceanic particulate matter. Nature 332, 341–343.

Blum, J.D., Erel, Y., 1997. Rb–Sr isotope systematics of a granitic soil chronosequence: the importance of biotite weathering. Geochim. Cosmochim. Acta 61, 3139–3204.

Blum, J.D., Erel, Y., Brown, K., 1993. 87Sr/86Sr ratios of Sierra Nevada stream waters: implications for relative mineral weathering rates. Geochim. Cosmochim. Acta 57, 5019–5025.

Bradtmiller, L.I., Anderson, R.F., Fleisher, M.Q., Burkle, L.H., 2007. Opal burial in the equatorial Atlantic Ocean over the last 30 ka: implications for glacial–interglacial changes in the ocean silicon cycle. Paleoceanography 22. doi:10.1029/2007PA001443,2007.

Bullen, T., White, A., Blum, A., Harden, J., Schulz, M., 1997. Chemical weathering of a soil chronosequence on granitoid alluvium: II. Mineralogical and isotopic constraints on the behavior of strontium. Geochim. Cosmochim. Acta 61, 291–306.

Carlson, T.N., Prospero, J.M., 1972. The large-scale movement of Saharan air outbreaks over the northern equatorial Atlantic. J. Appl. Meteor. 11, 283–297.

Chester, R., Hughes, M.J., 1967. A chemical technique for the separation of ferro-manganese minerals, carbonate minerals and absorbed trace elements from pelagic sediments. Chem. Geol. 2, 249–262.

Chiapello, I., Bergametti, G., Chatenet, B., Bousquet, P., Dulac, F., Santos Soares, E., 1997. Origins of African dust transported over the northeastern tropical Atlantic. J. Geophys. Res. 102, 13701–13709.

Chiapello, I., Bergametti, G., Gomes, L., Chatenet, B., Dulac, F., Pimenta, J., Santos Soares, E., 1995. An additional low layer transport of Sahelian and Saharan dust over the northeastern tropical Atlantic. Geophys. Res. Lett. 22, 3191–3194.

Claussen, M., Kubatzki, C., Brovkin, V., Ganapolski, A., Hoelzmann, P., Pachur, H.-J., 1999. Simulation of an abrupt change in Saharan vegetation in the mid-Holocene. Geophys. Res. Lett. 26, 2037–2040.

Colin, C., Turpin, L., Blamart, D., Frank, N., Kissel, C., Duchamp, S., 2006. Evolution of weathering patterns in the Indo-Burman Ranges over the last 280 kyr: effects of sediment provenance on 87Sr/86Sr ratios tracer. Geochem. Geophys. Geosys. 7, Q03007. doi:10.1029/2005GC000962.

Cullen, H.M., deMenocal, P.B., Hemming, S., Hemming, G., Brown, F.H., Guilderson, T., Sirocko, F., 2000. Climate change and the collapse of the Akkadian empire: evidence from the deep sea. Geology 28, 379–382.

Dasch, E.J., 1969. Strontium isotopes in weathering profiles, deep-sea sediments, and sedimentary rocks, Geochim. Cosmochim. Acta 33, 1521–1552.

deMenocal, P., Ortiz, J., Guilderson, T., Adkins, J., Sarnthein, M., Baker, L., Yarusinsky, M., 2000a. Abrupt onset and termination of the African Humid Period: Rapid climate responses to gradual insolation forcing. Quat. Sci. Rev. 19, 347–361.

deMenocal, P., Ortiz, J., Guilderson, T., Sarnthein, M., 2000b. Coherent high- and low-latitude climate variability during the Holocene warm period. Science 288, 2198–2202.

Eisenhauer, A., Meyer, H., Rachold, V., Tütken, T., Wiegand, B., Hansen, B.T., Spielhagen, R.F., Lindemann, F., Kassens, H., 1999. Grain size separation and sediment mixing in Arctic Ocean sediments: evidence from the strontium isotope systematic. Chem. Geol. 158, 173–188.

Franzese, A.M., Hemming, S.R., Goldstein, S.L., Anderson, R.F., 2006. Reduced Agulhas Leakage during the Last Glacial Maximum inferred from an integrated provenance and flux study. Earth Planet. Sci. Lett. 250, 72–88.

Gasse, F., 2000. Hydrological changes in the African tropics since the Last Glacial Maximum. Quat. Sci. Rev. 19, 189–211.

Gasse, F., Stabell, B., Fourtanier, E., van Iperen, Y., 1989. Freshwater diatom influx in intertropical Atlantic: relationships with continental records from Africa. Quat. Res. 32, 229–243.

Gasse, F., Téhet, R., Durand, A., Gibert, E., Fontes, J.-C., 1990. The arid-humid transition in the Sahara and the Sahel during the last deglaciation. Nature 346, 141–146.

Gasse, F., Van Campo, E., 1994. Abrupt post-glacial climate events in West Asia and North Africa monsoon domains. Earth Planet. Sci. Lett. 126, 435–456.

Glaccum, R.A., Prospero, J.M., 1980. Saharan aerosols over the tropical North Atlantic — Mineralogy. Mar. Geol. 37, 295–321.

Goldstein, S.L., O'Nions, R.K., Hamilton, P.J., 1984. A Sm–Nd isotopic study of atmospheric dusts and particulates from major river systems. Earth Planet. Sci. Lett. 70, 221–236.

Grousset, F.E., Biscaye, P.E., 2005. Tracing dust sources and transport patterns using Sr, Nd, and Pb isotopes. Chem. Geol. 222, 149–167.

Grousset, F.E., Parra, M., Bory, A., Martinez, P., Bertrand, P., Shimmield, G., Ellam, R.M., 1998. Saharan wind regimes traced by the Sr–Nd isotopic composition of subtropical Atlantic sediments: Last Glacial Maximum vs today. Quat. Sci. Rev. 17, 395–409.

Grousset, F.E., Rognon, P., Coudé-Gaussan, G., Pédemay, P., 1992. Origins of peri-Saharan dust deposits traced by their Nd and Sr isotopic composition. Palaeogeog. Palaeoclimat. Palaeoecol. 93, 203–212.

Haslett, S., Davies, C.F.C., 2006. Late Quaternary climate-ocean changes in western North Africa: offshore geochemical evidence. Trans. Inst. Br. Geogr. 31, 34–52.

Hemming, S.R., 2007. Terrigenous sediments. In: Elias, S.A. (Ed.), Encyclopedia of Quaternary Science, vol. 3. Elsevier, Oxford, pp. 1776–1785.

Hoelzmann, P., Jolly, D., Harrison, S.P., Laarif, F., Bonnefille, R., Pachur, H.-J., 1998. Mid-Holocene land-surface conditions in northern Africa and the Arabian Peninsula: a data set for the analysis of biogeophysical feedbacks in the climate system. Global Biogeochem. Cycles 12, 35–51.

Hooghiemstra, H., Lezine, A.M., Leroy, S.A.G., Dupont, L., Marret, F., 2006. Late Quaternary palynology in marine sediments: a synthesis of the understanding of pollen distribution patterns in the NW African setting. Quat. Int. 148, 29–44.

Jacobsen, S.B., Wasserburg, G.J., 1980. Sm–Nd isotopic evolution of chondrites. Earth Planet. Sci. Lett. 50, 139–155.

John, C.M., 2004. Plotting and analyzing data trends in ternary diagrams made easy. Eos, Trans. AGU 85, 158. doi:10.1029/2004EO160004.

Jolly, D., Prentice, I.C., Bonnefille, R., Ballouche, A., Bengo, M., Brenac, P., Buchet, G., Burney, D., Cazet, J.-P., Cheddadi, R., Edorh, T., Elenga, H., Elmoutaki, S., Guiot, J., Laarif, F., Lamb, H., Lezine, A.-M., Maley, J., Mbenza, M., Peyron, O., Reille, M., Reynaud-Farrera, I., Riollet, G., Ritchie, J.C., Roche, E., Scott, L., Ssemmanda, I., Straka, H., Umer, M., Van Campo, E., Vilimumbalo, S., Vincens, A., Waller, M., 1998. Biome reconstruction from pollen and plant macrofossil data for Africa and the Arabian peninsula at 0 and 6000 years. J. Biogeog. 25, 1007–1027.

Jullien, E., Grousset, F., Malaizé, B., Duprat, J., Sanchez-Goni, M.F., Eynaud, F., Charlier, K., Schneider, R., Bory, A., Bout, V., Flores, J.A., 2007. Low-latitude “dusty events” vs. high-latitude “icy Heinrich events”. Quat. Res. 68, 379–386.

Jung, S.J.A., Davies, G.R., Ganssen, G.M., Kroon, D., 2004. Stepwise Holocene aridification in NE Africa deduced from dust-borne radiogenic isotope records. Earth Planet. Sci. Lett. 221, 27–37.
Kelley, K.A., Plank, T., Ludden, J., Staudigel, H., 2003. Composition of altered oceanic crust at ODP Sites 801 and 1149. Geochem. Geophys. Geosys. 4. doi:10:1029/2002GC000435.
Kohfeld, K.E., Harrison, S.P., 2001. DIRTMAP: the geological record of dust. Earth-Sci. Rev. 54, 81–114.
Krastel, S., Hanebuth, T.J.J., Antobreh, A.A., Henrich, R., Holz, C., Kölling, M., Schultz, H.D., Wien, K., Wynn, R.B., 2004. Cap Timiris Canyon: a newly discovered channel system offshore of Mauritania. Eos Trans. AGU 85, 417–432. doi:10.1029/2004EO420001.
Kröpelin, S., Verschuren, D., Lézine, A.-M., Eggermont, H., Cocquyt, C., Francus, P., Cazet, J.-P., Fagot, M., Rumes, B., Russell, J.M., Darius, F., Conley, D.J., Schuster, M., von Suchodoletz, H., Engstrom, D.R., 2008. Climate-driven ecosystem succession in the Sahara: the past 6000 years. Science 320, 765–768.
Lange, C.B., Romero, O.E., Wefer, G., Gabric, A.J., 1998. Offshore influence of coastal upwelling off Mauritania, NW Africa, as recorded by diatoms in sediment traps at 2195 m water depth. Deep-Sea Res. I 45, 985–1013.
Latimer, J.C., Filippelli, G.M., Hendy, I.L., Gleason, J.D., Blum, J.D., 2006. Glacial-interglacial terrigenous provenance in the southeastern Atlantic Ocean: the importance of deep-water sources and surface currents. Geology 34, 545–548.
Matthewson, A.P., Shimmield, G.B., Kroon, D., Fallick, A.E., 1995. A 300 kyr high-resolution aridity record of the North African continent. Paleoceanography 10, 677–692.
McIntosh, S.K., McIntosh, R.J., 1983. Current directions in West African prehistory. Ann. Rev. Anthropol. 12, 215–258.
McLennan, S.M., 1993. Weathering and global denudation. J. Geology 101, 295–303.
McLennan, S.M., 2001. Relationships between the trace element composition of sedimentary rocks and upper continental crust. Geochem. Geophys. Geosys. 2 2000GC000109.
McLennan, S.M., Hemming, S., McDaniel, D.K., Hanson, G.N., 1993. Geochemical approaches to sedimentation, provenance, and tectonics. Geol. Soc. Am. Spec. Pap. 284, 21–40.
McLennan, S.M., Taylor, S.R., McCulloch, M.T., Maynard, J.B., 1990. Geochemical and Nd–Sr isotopic composition of deep-sea turbidites: crustal evolution and plate tectonic associations. Geochim. Cosmochim. Acta 54, 2015–2050.
Mittelstaedt, E., 1991. The ocean boundary along the Northwest African coast: circulation and oceanographic properties at the sea surface. Prog. Oceanogr. 26, 307–355.
Moreno, T., Querol, X., Castillo, S., Alastuey, A., Cuevas, E., Herrmann, L., Mounkaila, M., Elvira, J., Gibbons, W., 2006. Geochemical variations in aeolian mineral particles from the Sahara-Sahel Dust Corridor. Chemosphere 65, 261–270.
Müller, P.J., Fischer, G., 2001. A 4-year sediment trap record of alkenones from the filamentous upwelling region off Cape Blanc, NW Africa and a comparison with distributions in underlying sediments. Deep-Sea Res. I 48, 1877–1903.
Murray, R.W., Miller, D.J., Kryc, K.A., 2000. Analysis of major and trace elements in rocks, sediments, and interstitial waters by inductively coupled plasma-atomic emission spectrometry (ICP-AES), ODP Tech. Note 29. http://www-odp.tamu.edu/publications/tnotes/tn29/INDEX.HTM.
Nakai, S., Halliday, A.N., Rea, D.K., 1993. Provenance of dust in the Pacific Ocean. Earth Planet. Sci. Lett. 119, 143–157.
Nesbitt, H.W., Young, G.M., 1984. Prediction of some weathering trends of plutonic and volcanic rocks based on thermodynamic and kinetic considerations. Geochim. Cosmochim. Acta 48, 1523–1534.
Pettke, T., Halliday, A.N., Hall, C.M., Rea, D.K., 2000. Dust production and deposition in Asia and the north Pacific Ocean over the past 12 Myr. Earth Planet. Sci. Lett. 178, 397–413.
Pokras, E.M., Mix, A.C., 1985. Eolian evidence for spatial variability of late Quaternary climates in tropical Africa. Quat. Res. 24, 137–149.
Prospero, J.M., Ginoux, P., Torres, O., Nicholson, S.E., Gill, T.E., 2002. Environmental characterization of global sources of atmospheric soil dust identified with the Nimbus 7 Total Ozone Mapping Spectrometer (TOMS) absorbing aerosol product. Rev. Geophys. 40, 1002. doi:10.1029/2000RG000095.
Prospero, J.M., Lamb, P.J., 2003. African droughts and dust transport to the Caribbean: climate change implications. Science 302, 1024–1027.
Prospero, J.M., Nees, R.T., 1977. Dust concentration in the atmosphere of the equatorial North Atlantic: possible relationship to the Sahelian drought. Science 196, 1196–1198.
Prospero, J.M., Nees, R.T., 1986. Impact of the North African drought and El Niño on mineral dust in the Barbados trade winds. Nature 320, 735–738.
Ritchie, J.C., Eyles, C.H., Haynes, C.V., 1985. Sediment and pollen evidence for an early to mid-Holocene humid period in the eastern Sahara. Nature 330, 645–647.
Ruddiman, W., Sarnthein, M., Baldauf, J., Backman, J., Bloemendal, J., Curry, W., Farrimond, P., Faugeres, J.C., Janacek, T., Katsura, Y., Manivit, H., Mazzulo, J., Mienert, J., Pokras, E., Raymo, M., Schultheiss, P., Stein, R., Tauxe, L., Valet, J.-P., Weaver, P., Yasuda, H., 1988. Site 658. Proc. Ocean Drill. Program Init. Rep. 108, 105–137.
Ruddiman, W.F., 1997. Tropical Atlantic terrigenous fluxes since 25,000 yrs B.P. Mar. Geol. 136, 189–207.
Russell, J., Talbot, M.R., Haskell, B.J., 2003. Mid-holocene climate change in Lake Bosumtwi. Ghana, Quat. Res. 60, 133–141.
Rutberg, R.L., Goldstein, S.L., Hemming, S.R., Anderson, R.F., 2005. Sr isotope evidence for sources of terrigenous sediment in the southeast Atlantic Ocean: is there increased available Fe for enhanced glacial productivity? Paleoceanography 20, PA1018.
Sarnthein, M., Thiede, J., Pflaumann, U., Erlenkeuser, H., Fütterer, D., Koopmann, B., Lange, H., Seibold, E., 1982. Atmospheric and oceanic circulation patterns off Northwest Africa during the past 25 million years. In: von Rad, U., Hinz, K., Sarnthein, M., Seibold, E. (Eds.), Geology of the Northwest African Continental Margin. Springer-Verlag, New York, pp. 545–604.
Sarnthein, M., Tiedemann, R., 1989. Toward a high-resolution stable isotope stratigraphy of the last 3.4 million years: Site 658 and 659 off Northwest Africa. Proc. ODP, Sci. Results 108, 167–185.
Schütz, L., Jaenicke, R., Pietrek, H., 1981. Saharan dust transport over the North Atlantic Ocean. Geol. Soc. Am. Spec. Pap. 186, 87–100.
Sirocko, F., Garbe-Schönberg, D., Devey, C., 2000. Processes controlling trace element geochemistry of Arabian Sea sediments during the last 25,000 years. Glob. Planet. Change 26, 217–303.
Street, F.A., Grove, A.T., 1979. Global maps of lake-level fluctuations since 30,000 yr B.P. Quat. Res. 12, 83–118.
Stuut, J.-B., Zabel, M., Ratmeyer, V., Helmke, P., Schefuß, E., Lavik, G., Schneider, R., 2005. Provenance of present-day eolian dust collected off NW Africa. J. Geophys. Res. 110, D04202. doi:10.1029/2004JD005161.
Tateo, F., Sabbadini, R., Morandi, N., 2000. Palygorskite and sepiolite occurence in Pliocene lake deposits along the River Nile: evidence of an arid climate. J. Afr. Earth Sci. 31, 633–645.
Taylor, S.R., McLennan, S.M., 1985. The Continental Crust: Its Composition and Evolution. Blackwell Scientific Publications, Oxford.
Taylor, S.R., McLennan, S.M., McCulloch, M.T., 1983. Geochemistry of loess, continental crustal composition and crustal model ages. Geochim. Cosmochim. Acta 47, 1897–1905.
Teng, F.-Z., McDonough, W.W., Rudnick, R.L., Dalpé, C., Tomascak, P.B., Chappell, B.W., Gao, S., 2004. Lithium isotopic composition and concentration of the upper continental crust. Geochim. Cosmochim. Acta 68, 4167–4178.
Tjallingii, R., Claussen, M., Stuut, J.-B.W., Fohlmeister, J., Jahn, A., Bickert, T., Lamy, F., Röhl, U., 2008. Coherent high- and low-latitude control of the Northwest African hydrological balance. Nature Geosci. 1, 670–675. doi:10.1038/ngeo289.
Tütken, T., Eisenhauer, A., Wiegand, B., Hansen, B.T., 2002. Glacial-interglacial cycles in Sr and Nd isotopic composition of Arctic marine sediments triggered by the Svalbard/Barents Sea ice sheet. Mar. Geol. 182, 351–372.
Walter, H.J., Hegner, E., Diekmann, B., Kuhn, G., Rutgers van de loeff, M.M., 2000. Provenance and transport of terrigenous sediment in the south Atlantic Ocean and their relations to glacial and interglacial cycles: Nd and Sr isotopic evidence. Geochim. Cosmochim. Acta 64, 3813–3827.
Weldeab, S., Emeis, K.-C., Hemleben, C., Vennemann, T.W., Schulz, H., 2002. Sr and Nd isotope composition of Late Pleistocene sapropels and nonsapropelic sediments from the Eastern Mediterranean Sea: implications for detrital flux and climatic conditions in source areas. Geochim. Cosmochim. Acta 66, 3585–3598.
Zabel, M., Wagner, T., deMenocal, P., 2003. Terrigenous signals in sediments of the low-latitude Atlantic — indications to environmental variation during the late Quaternary: Part II: Lithogenic matter. In: Wefer, G., Mulitza, S., Ratmeyer, V. (Eds.), The South Atlantic in the Late Quaternary: Reconstruction of Mass Budget and Current Systems. Springer-Verlag, New York. pp.
Zhao, M., Dupont, L., Eglinton, G., Teece, M., 2003. n-Alkane and pollen reconstruction of terrestrial climate and vegetation for N.W. Africa over the last 160 kyr. Org. Geochem. 34, 131–143.
Zühlsdorff, C., Wien, K., Stuut, J.-B.W., Henrich, R., 2007. Late Quaternary sedimentation within a submarine channel-levee system offshore Cap Timiris. Mauritania, Mar. Geol. 240, 217–234.